Available online at www.sciencedirect.com
SCIENCE DIRECT®
ELSEVIER
Solid-State Electronics 48 (2004) 1579–1586
SOLID-STATE ELECTRONICS
www.elsevier.com/locate/sse

Investigation of defect properties in $Cu(In,Ga)Se_2$ solar cells by deep-level transient spectroscopy

L.L. Kerr [a], Sheng S. Li [b,*], S.W. Johnston [c], T.J. Anderson [a], O.D. Crisalle [a], W.K. Kim [a], J. Abushama [c], R.N. Noufi [c]

[a] *Department of Chemical Engineering, University of Florida, Gainesville, FL 32611, USA*
[b] *Department of Electrical and Computer Engineering, Gainesville, FL 32611, USA*
[c] *National Renewable Energy Lab, Golden, CO 80401, USA*

Received 1 July 2003; received in revised form 1 January 2004
Available online 21 April 2004

The review of this paper was arranged by Prof. S. Cristoloveanu

Abstract

The performance of the chalcopyrite material $Cu(In,Ga)Se_2$ (CIGS) used as an absorber layer in thin-film photovoltaic devices is significantly affected by the presence of native defects. The deep-level transient spectroscopy (DLTS) technique is used in this work to characterize the defect properties, yielding relevant information about the defect types, their capture cross-sections, and energy levels and densities in the CIGS cells. Three solar cells developed using different absorber growth technologies were analyzed using DLTS, capacitance–voltage (C–V), and capacitance–temperature (C–T) techniques. It was found that CIS cells grown at the University of Florida exhibits a middle-gap defect level that may relate to the cell's low fill factor and open-circuit voltage values observed. A high efficiency ($\eta_c > 18\%$) CIGS cell produced by the National Renewable Energy Laboratory (NREL) was found to contain three minority-carrier (electron) traps and a 13% CIGS cell produced by the Energy Photovoltaics Inc. (EPV) exhibited one majority (hole) trap. The approach followed using the DLTS technique serves as a paradigm for revealing the presence of significant defect levels in absorber materials, and may be used to support the identification of remedial processing operations.
© 2004 Elsevier Ltd. All rights reserved.

1. Introduction

Chalcopyrite $CuInSe_2$ (CIS) and its alloy $Cu(In,Ga)Se_2$ (CIGS) in polycrystalline form hold great potential for photovoltaic device applications. Unlike conventional binary semiconductors (such as GaAs or ZnSe), it can tolerate a large range of anion-to-cation off-stoichiometry. This is important for cell fabrication since Cu-deficient and/or Indium deficient stoichiometries are stable and useful. This brings an advantage in terms of opportunities for bandgap engineering and defect chemistry modifications. The large composition homogeneity range and the deviation from stoichiometry in compound semiconductors such as CIGS are often attributed to antisite defects, vacancies, interstitials and defect clusters in the material. It is well known that CIS films can be produced in both p and n-type characteristics by the introduction of *native* defects with or without extrinsic impurities. However, the doping mechanism and point defect chemistry of CIS are not well understood at the fundamental level. Therefore, it is important to advance the understanding of these properties to further improve the cell efficiency and reduce the processing cost of solar cells. Deep-level defects play an important role in determining the recombination and trapping mechanisms (and hence the minority-carrier lifetimes) in CIGS solar cells.

Zhang [1] has calculated the transition energy for a large number of defects in CIS materials. However, there are some discrepancies between their calculations and

* Corresponding author. Tel./fax: +1-352-392-4937.
E-mail address: shengli@eng.ufl.edu (S.S. Li).

0038-1101/$ - see front matter © 2004 Elsevier Ltd. All rights reserved.
doi:10.1016/j.sse.2004.03.005

the experimental observations. For example, according to the photoluminesense spectroscopy measurements by Schön and Bucher [2], the In_{Cu} defect is a shallow donor with an ionization energy of $E_c - 0.2$ eV and the calculated energy level of In_{Cu} by Zhang [1] is $E_c - 0.5$ eV. In the first-principle calculations reported by Zhang [1] the anion site defect was neglected. However, many other researchers believe that the selenium vacancy V_{Se} is a shallow donor level with an energy level of $E_c - 0.06$ eV, and could lead to a significant lattice relaxation during the ionization process [3]. It has been found that the electronic and optical properties of CIGS film and the cell performance are significantly affected by the deep-level defects, as reported by the previous DLTS studies [4–7]. The energy levels and densities of deep-level defects are important input parameters for developing an accurate device model for the CIS-based solar cells. The deep-level transition spectroscopy (DLTS) technique is a powerful tool for determining the defect properties such as defect energy level, capture cross-section, and trap concentration in a semiconductor [8,9].

2. The experimental procedure

The DLTS technique is used to measure the transient capacitance change in CIS-based solar cells after deep-level traps in the space charge region are filled with either the majority or minority-carrier charges. More specifically, the density and energy level as well as the capture cross-section of these deep-level traps can be determined from the DLTS and C–V (capacitance versus voltage) measurements.

By scanning the capacitance change over a wide range of temperatures under different rate windows, the emission rate e_n as a function of inverse temperature T^{-1} can be obtained. From the Arrhenius plot, (i.e., ln $(T^2\tau)$ vs. T^{-1}, where $\tau = 1/e_p$) we can extract the activation energy E_a and the capture cross-section σ_n of the defect level [10]. The hole emission-rate is related to the capture cross-section and the activation energy of the trap level by:

$$e_p = \sigma_n v_{th} N_c \exp\left(-\frac{E_a}{kT}\right) \tag{1}$$

where v_{th} is the thermal velocity, σ_p is the hole capture cross section, and N_c is the effective density of the conduction band states. It is noted that if the capture cross-section for the trap is a thermally activated process [11], then it is related to temperature by the expression $\sigma_p = \sigma_\infty \exp(-\Delta E_o/kT)$, where σ_∞ is the hole capture cross section at T equal to infinity, and ΔE_o the capture cross section activation energy. The hole trap density, N_T, can be calculated by using the expression

$$N_T \approx \frac{2\Delta C}{C_0} N_a \tag{2}$$

where N_a is the net hole concentration; ΔC is the capacitance change due to the emission of charge carriers from the trap level, which is proportional to the trap concentration; and C_0, the zero-bias capacitance which can be determined from the capacitance versus temperature (C–T) scan at the corresponding DLTS peak temperature. Eq. (2) is valid for $N_T < N_a$. Finally, the net hole concentration N_a in a p-type CIGS absorber layer can be determined via C–V measurements.

3. Results and discussion

DLTS studies were conducted on three types of thin-film photovoltaic cells:

(i) CIS cells (denoted as "UF CIS cells") developed by the University of Florida CIS team using a bilayer precursor process.
(ii) CIGS cells (denoted as "EPV CIGS cells") developed by the Energy Photovoltaics Inc. (EPV) using a physical-vapor deposition process.
(iii) CIGS cells (denoted as "NREL CIS cell") developed by the National Renewable Energy Laboratory (NREL) using a three-stage precursor process.

Detailed description of the growth, fabrication and characterization for the above CIS and CIGS cells are discussed as follows:

3.1. Analysis of UF CIS cells

3.1.1. Background and material growth procedure

An alternative growth process for $CuInSe_2$ (CIS) films has been developed by the research team at the University of Florida (UF) in Gainesville, Florida. In this approach, a binary two-layer precursor Cu–Se/In–Se film is first deposited on a Mo-coated soda lime glass substrate at low temperature (150–200 °C) using the plasma migration enhanced epitaxy (PMEE) technique (a variant of molecular-beam deposition) [12]. Then rapid thermal processing (RTP) under a controlled Se ambient is used to synthesize single-phase $CuInSe_2$ (CIS) film. A schematic of the proposed two-layer precursor structure for growing α-CIS film is shown in Fig. 1, where the

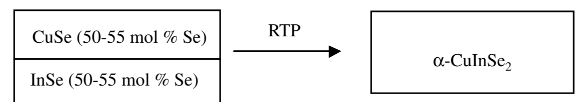

Fig. 1. The precursor structure consisting of stacked metal–Se layers subjects to rapid-thermal processing (RTP) to produce a single-phase α-CIS film.

bilayer precursor consists of a slightly Se-rich In–Se binary layer deposited at low temperature on a Mo-coated soda-lime glass substrate, followed by the deposition of a Se-rich Cu–Se binary layer.

This composition of the bilayer precursor structure shown in Fig. 1 where each layer has a slightly selenium-rich composition of 50–55 mol% was conceived after an examination of the Cu–In–Se phase diagram for conditions that show α-$CuInSe_2$ in equilibrium with a liquid phase at low temperature. More precisely, the precursor layer compositions were selected based on the likelihood of forming the desired liquid phase while avoiding compounds that have a high melting temperature. Fig. 2 shows the isothermal equilibrium composition diagram for the ternary Cu–In–Se system at 500 °C [13]. The α-$CuInSe_2$ phase is seen to lie on the tie line connecting the In_2Se_3 and Cu_2Se phases, and it shows a solid solution range of several mole percent units. Note that a low-temperature single-phase Se-rich liquid solution is located near the Se corner of the phase diagram. The triangle connecting the α-$CuInSe_2$ phase boundary with the Se corner represents the two-phase region consisting of an α-$CuInSe_2$ phase and a Se-rich liquid phase, which represents the target for the desired overall film composition. The phase diagram also indicates that the Se-rich liquid phase can exist at a temperature as low as 211 °C [13]. It is also suggested that the synthesized CIS will be Se-rich and that excess Se can easily volatilize during the annealing process. Starting from a precursor where the binary metal–Se layers are in contact promises to avoid reactions that yield high melting temperature compounds, and to increase grain size through a liquid phase assisted growth mechanism. The rapid thermal processing mitigates undesirable solid-to-solid transformations that are predicted to occur at low temperatures.

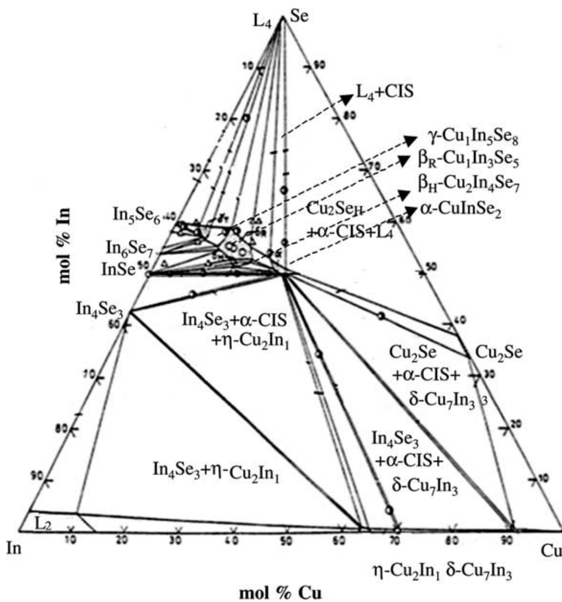

Fig. 2. Isothermal composition phase diagram of the Cu–In–Se system at 500 °C.

3.1.2. I–V and DLTS measurements

Fig. 3 shows the I–V curve for a UF CIS cell with 5% AM1.5G conversion efficiency, open-circuit voltage $V_{oc} = 0.296$ V, and fill factor F.F. = 49.54%. The short-circuit current density, J_{sc}, for this cell is 34.65 mA/cm^2, which is an excellent value for CIS cells. The high short-circuit current indicates long minority-carrier lifetime and diffusion length in the CIS film, while low fill factor may be attributed to the high series resistance in the CIS absorber. This could be improved by adjusting the Cu:In:Se composition ratio, especially the Cu to In ratio, and by creating a composition gradient to achieve bandgap grading. The low V_{oc} value may be attributed to the low hole concentration and high series resistance and mid-gap defect density in the CIS absorber.

The DLTS and C–V measurements were performed on the UF CIS cells to characterize the deep-level defects in the films. Fig. 4 shows the C–V data on the 5% cell obtained at different temperatures. The average hole concentration determined from the C–V plots was found to be around 10^{15} cm^{-3}. The C–V data were measured on the same cell that was used in the DLTS measurements. From the C–T measurements, values of the zero-biased capacitance C_0 corresponding to the DLTS peak temperatures at 150, 200, 290, and 300 K were found to be 28.6, 28.8, 34.4, and 37.7 pF, respectively.

Fig. 5(a) shows the DLTS spectra for this CIS cell obtained using a reverse bias voltage, $V_R = -0.5$ V, a trap-filling pulse of 0.4 V, and a saturation pulse width of 10 ms. From these DLTS data a deep-level majority

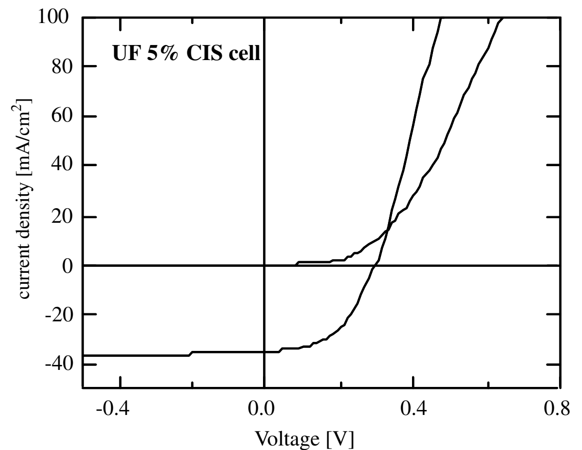

Fig. 3. The dark and photo-current–voltage (I–V) curves for the UF CIS cell fabricated from the binary bilayer process and RTP.

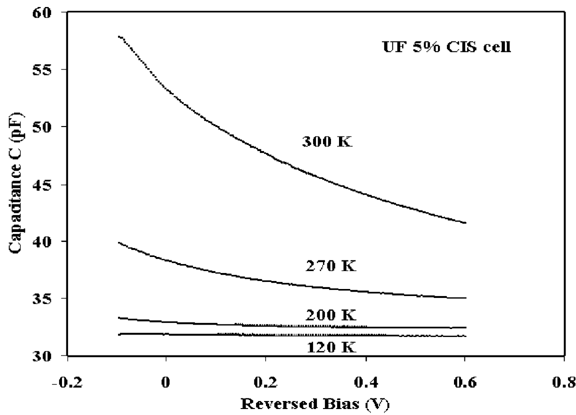

Fig. 4. The capacitance–voltage (C–V) curves for the UF CIS cell measured at different temperatures.

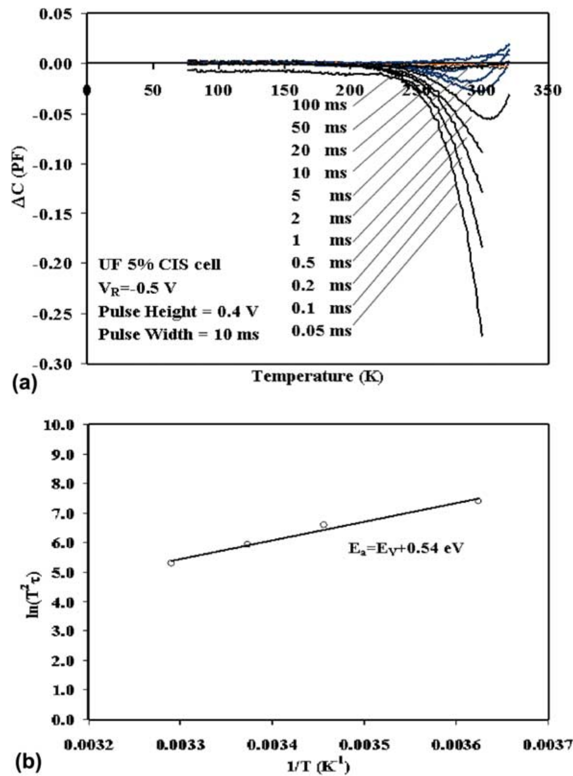

Fig. 5. (a) The DLTS scans for the UF CIS cell at different rate windows and at a reverse bias $V_R = -0.5$ V, a pulse height of 0.4 V, and a pulse width of 10 ms. (b) Arrhenius plot obtained from the DLTS scans shown in (a).

carrier trap (hole trap) was obtained at a temperature of approximately 290 K. Fig. 5(b) shows the corresponding Arrhenius plot, yielding an activation energy $E_a = E_v + 0.54$ eV. The average hole density determined from the C–V measurements was found to be 2×10^{15} cm^{-3}. From the C–T and C–V data, the net trap density, N_T, was found to be 4.6×10^{12} cm^{-3}, which is relatively low compared to the net hole density in the film. This could explain the high J_{sc} observed in this cell.

To detect the possible minority-carrier traps, a small forward bias was applied to this CIS cell to fill the minority-carrier traps at room temperature, and the cell was then cooled down to 77 K to freeze out all the minority-carrier traps. The cell was then heated up, and a pulse amplitude equal to 0.7 V, a reverse set-off voltage of −0.5 V and a saturation pulse width of 10 ms were applied to the device to observe the capacitance change due to the minority-carrier emission. The results are shown in Fig. 6(a), where a minority-carrier (electron) trap peak was observed at a temperature of approximately 200 K in addition to the majority carrier trap depicted in the previous paragraph. The companion Arrhenius plots for the minority-carrier trap peak E_1 and for the majority-carrier trap peak E_2 given in Fig. 6(b) reveal that the activation energy for the minority (electron) trap is $E_1 = E_c - 0.52$ eV and the trap density was estimated to be 1.3×10^{12} cm^{-3}.

In addition to the standard DLTS scans described above, we also performed optical DLTS measurements on the UF CIS cell. The optical DLTS technique is to

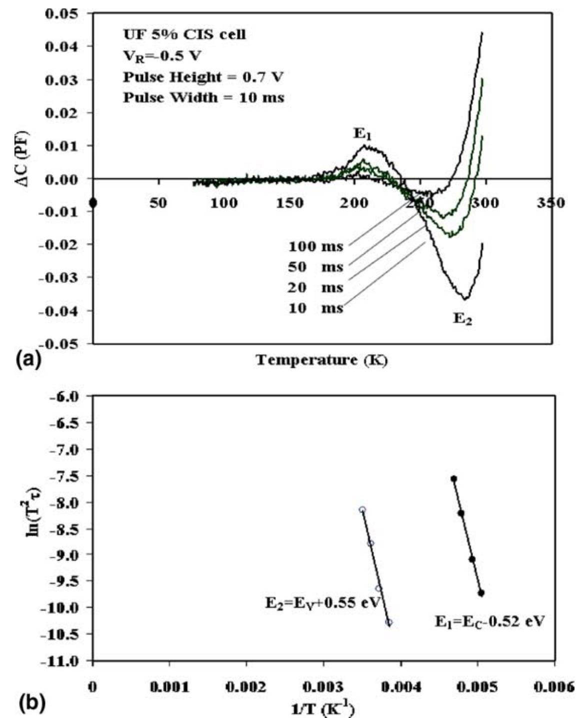

Fig. 6. (a) The DLTS scans for the UF CIS cell at a reverse bias $V_R = -0.5$ V, a pulse height of 0.7 V, and a pulse width of 10 ms, and (b) the Arrhenius plots obtained from the DLTS scan shown in (a).

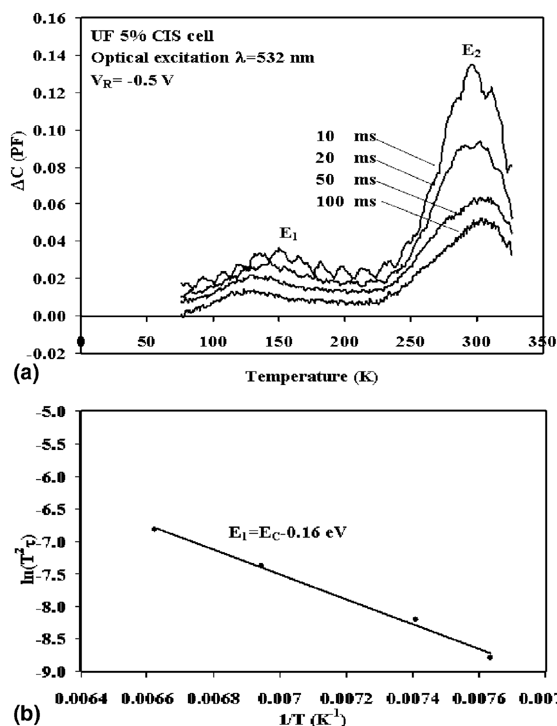

Fig. 7. (a) The optical DLTS scans for the UF CIS cell measured at a reverse bias of $V_R = -0.5$ V, $\lambda = 532$ nm, and pulse width of 10 ms, and (b) the Arrhenius plot obtained from the DLTS scans shown in (a).

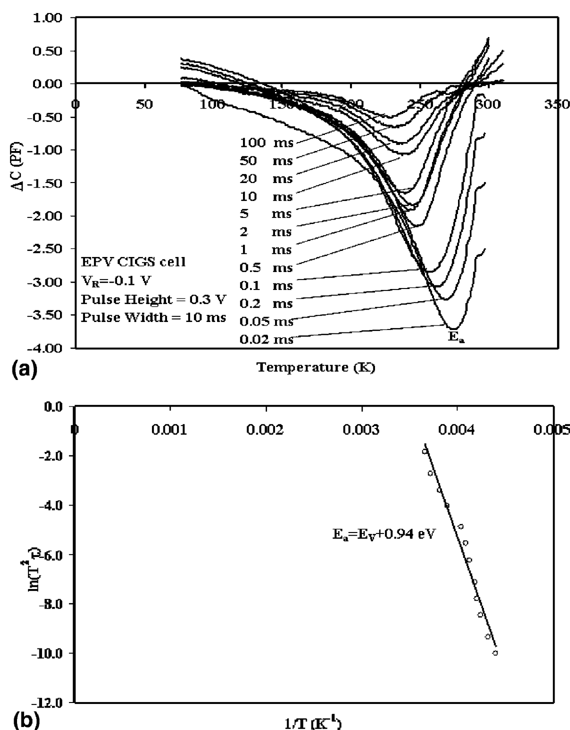

Fig. 8. (a) The DLTS scans for the EPV CIGS cell at a reverse bias of $V_R = -0.1$ V, a pulse height of 0.3 V, and a pulse width of 10 ms, and (b) the Arrhenius plot obtained from the DLTS scans shown in (a).

use optical pulses to substitute the electrical pulses, to fill the minority-carrier trap levels and hence is used mainly to reveal the minority traps [14,15]. A laser beam with wavelength of 532 nm was used to inject the minority-carriers in this CIS cell with a reverse bias of −0.5 V. Results of the optical DLTS scans are shown in Fig. 7(a), where two minority-carrier traps with activation energies of E_1 and E_2 were observed. As shown in the Arrhenius plot of Fig. 7(b), the activation energy calculated for the E_1 electron trap is $E_c - 0.16$ eV. The activation energy at 300 K for a deeper electron trap could not be estimated since the shift of DLTS peaks does not follow the general trend (i.e., the shorter the rate window, the higher the temperature at which the peak occurs).

3.2. Analysis of EPV CIGS cells

To compare the defect properties of UF CIS cells with CIGS cells produced by other NREL CIS TFPPP team members, the CIGS cells produced by the Energy Photovoltaics Inc. (EPV) were also analyzed. The CIGS cell provided by EPV has a conversion efficiency of around 13% AM1.5G. The absorber films were grown by co-deposition in a proprietary physical vapor deposition system. Fig. 8(a) shows the DLTS spectra measured for a typical EPV CIGS cell, obtained using a reverse bias $V_R = -0.1$ V, a trap-filling pulse of 0.3 V, and a saturation pulse width of 10 ms. The EPV CIGS cell shows a deep majority-carrier (hole) trap at a temperature approximately equal to 270 K. The DLTS peak shifts to higher temperatures with shorter rate windows. The activation energy calculated from the Arrhenius plot of Fig. 8(b) for this hole trap is $E_a = E_v + 0.94$ eV. The average hole density obtained from the C–V data at 270 K is 3×10^{15} cm^{-3}. Using the C–T data the zero biased capacitance value, C_0, was found equal to 301 pF and from Eq. (2) the hole trap density N_T was found equal to 6.5×10^{13} cm^{-3}.

3.3. Analysis of NREL CIGS cells

A high efficiency CIGS cell prepared at NREL using the three-stage process [16] in a physical vapor deposition system was also studied. In the first processing stage, a precursor $(In,Ga)_2Se_3$ layer is formed by the co-evaporation of In, Ga, and Se from elemental sources while holding the substrate at a temperature of approximately 260 °C. In the second stage, Cu and Se are co-evaporated to bring the overall composition to a

near Cu-rich regime (corresponding to an elemental ratio Cu/(In+Ga) ranging from 0.97 to 1.08) at 560 °C. Before starting the third stage, the substrate is held under a Se flux while the temperature is ramped up to a new target. The third stage then commences, where In, Ga, and Se were added in an amount equal to one-ninth of the first stage to bring the overall composition back to a Cu-poor range at the substrate temperature used in the second stage. Finally, the substrate is cooled down to 350 °C and held under a Se flux for 20 min. The process requires very precise control of the source fluxes.

The NREL CIGS cell subjected to DLTS analysis has a total-area conversion efficiency of 19.2% (AM1.5G). Fig. 9(a) shows the results of a DLTS scan carried out using an electrical pulse with an amplitude equal to 0.4 V, and a reverse set-off voltage of −0.5 V. The figure reveals a minority-carrier trap peak at near 100 K. From the companion Arrhenius plot of Fig. 9(b) the activation energy was found to be $E_1 = E_c - 0.07$ eV and the trap density was estimated to be $N_T = 4.2 \times 10^{13}$ cm^{-3}. The DLTS scan performed at higher temperatures showed another possible peak; however, the activation energy for this trap could not be resolved by heating the sample above 300 K due possibly to the large temperature dependence of the capture cross-section for this trap.

From the results of DLTS scans on the NREL CIGS cell, it is noted that the minority-carrier traps are likely the dominant traps in this cell. To detect other possible minority traps, a small forward bias of 0.1 V was applied at room temperature, and the cell was then cooled down to 77 K to freeze the minority-carriers. The sample was then heated with $V_R = -0.5$ V, a trap-filling pulse amplitude of 0.7 V, and a saturation pulse width of 10 ms to observe the capacitance change due to the minority-carrier emission. The DLTS results of Fig. 10(a) shows three minority-carrier traps, and features the emergence of a small peak around 250 K, which was not apparent in the previous DLTS spectra obtained under a 0.4 V pulse amplitude. The Arrhenius plot of Fig. 10(b) shows that the activation energy for the electron trap at 80 K is $E_1 = E_c - 0.14$ eV, and the trap density is estimated to be 2.54×10^{13} cm^{-3}. The activation energy at 335 K could not be estimated since the peak shift does not follow the general trend, as discussed before. The minority-carrier traps observed in the NREL CIGS cell do not have significant effects on the performance of NREL CIGS cell since the conversion efficiency in this cell is very high compared to other CIGS cells reported in the literature. The densities of these minority traps are not high enough to affect the

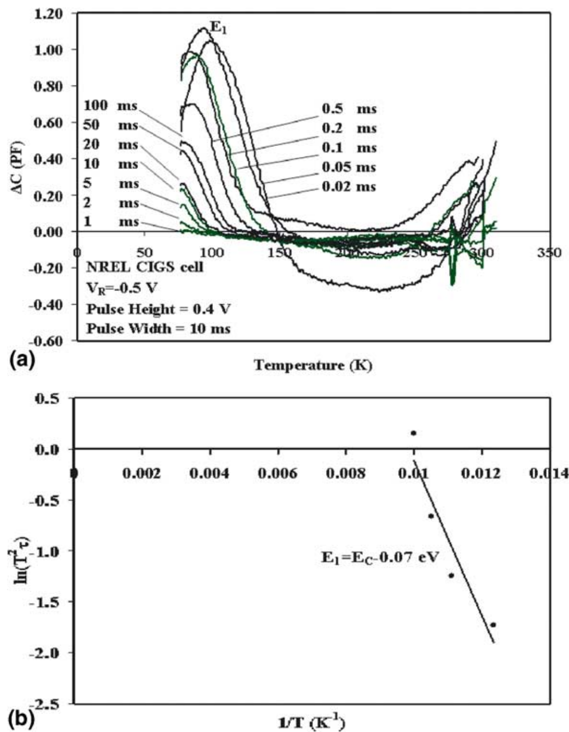

Fig. 9. (a) The DLTS scans for the NREL CIGS cell measured at a reverse bias $V_R = -0.5$ V, a pulse height of 0.4 V, and a pulse width of 10 ms, and (b) the Arrhenius plot obtained from the DLTS scans shown in (a).

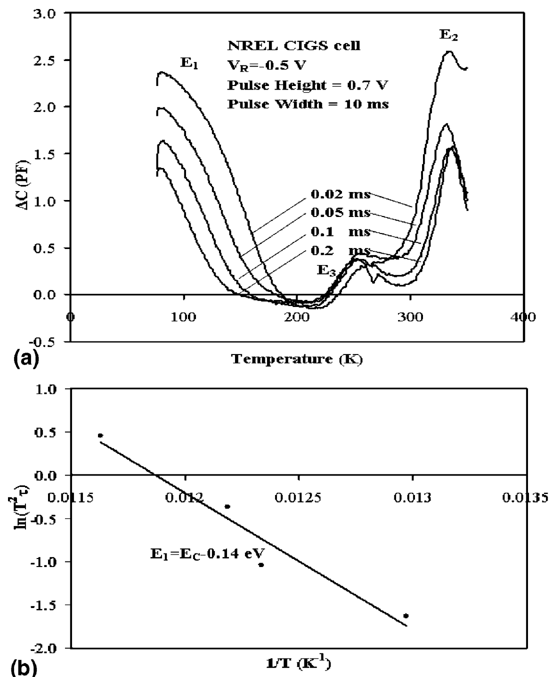

Fig. 10. (a) The DLTS scans for the NREL CIGS cell under forward bias injection ($V_F = 0.1$ V) and at a reverse bias $V_R = -0.5$ V, a pulse height of 0.7 V, and a pulse width of 10 ms, and (b) the Arrhenius plot obtained from the DLTS scans shown in (a).

minority-carrier lifetimes and hence the performance of this cell.

4. Conclusions

The DLTS and C–V measurements have been performed on three different CIS and CIGS-thin film solar cells fabricated by UF, EPV, and NREL, respectively to characterize the deep-level defects in these cells. The defect activation energies and trap densities were determined. Table 1 summarizes the DLTS data for the UF CIS cell prepared by using a binary bilayer precursor process followed by RTP. A mid-gap hole-trap and three electron traps were detected in this cell. The mid-gap hole-trap was found to be the dominant deep-level defect in this cell. Since the density of this defect is very low ($\approx 10^{12}$ cm^{-3}), value of J_{sc} remained quite high for the UF CIS cell. The observed low V_{oc} in this cell is attributed to the low hole density and high series resistance in the CIS absorber. Therefore, to further improve the cell performance, it is necessary to improve the junction quality by using bandgap gradient and eliminating defects in the CIS films. One method worthy of consideration is to intentionally dope the film with sodium. Sodium can reduce the number of mid-gap states especially those that act as minority-carrier traps as evidenced by the PL [17] and DLTS [7] measurements. We believe that the doped sodium will enter the indium site and substitute copper to form Na_{In} defects, and therefore reduce the grain boundary energy barrier and remove the mid-gap states. Adding Ga or S to create a band-gap gradient and obtain a final film with a $Cu(In_{1-x}Ga_x)(Se,S)_2$ composition with wider bandgap and adjusting the Cu:In:Se composition ratio could be a viable approach to achieve this goal. The Ga will segregate at the back surface of the absorber and create a bandgap grading in the CIGS absorber layer.

The DLTS analysis of the EPV CIGS cell revealed a majority carrier (hole) trap with an activation energy of $E_v + 0.94$ eV and trap density of 6.5×10^{13} cm^{-3}. The NREL CIGS cell showed three minority-carrier traps, with one dominant shallow-trap with activation energy of $E_c - 0.067$ eV and trap density of 4.2×10^{13} cm^{-3}. A summary of key results obtained from the DLTS analysis for the EPV and NREL CIGS cells are listed in Table 2. From the DLTS analysis on the three types of CIS and CIGS cells depicted in this work we have found several deep-level defects including both the minority and majority carrier traps in these cells. However, it is difficult to assign these trap levels to certain defect origins reported in the literature with similar activation energy without further evidence and confirmation by other diagnostic techniques. It is worth noting that V_{Se} and In_{Cu} are the two main donor levels, and Cu_{In} is the main mid-gap recombination center in CIGS films, as reported in the literature [1,3]. Additional experimental works are needed to assign the possible physical origin of the defect levels observed in our DLTS measurements. The free energy associated with the formation of

Table 1
Summary of the DLTS and C–V analysis for the UF CIS cell

	$V_R = -0.5$ V, $V_H = 0.4$ V, $W = 10$ ms	$V_R = -0.5$ V, $V_H = 0.7$ V, $W = 10$ ms		Optical DLTS $V_R = -0.5$ V, $\lambda = 532$ nm	
Approximate peak temperature (K)	290	290	200	150	300
DLTS peak sign	–	–	+	+	+
Trap carrier type	Majority	Majority	Minority	Minority	Minority
Trap activation energy E_a (eV)	$E_v + 0.54$	$E_v + 0.55$	$E_c - 0.52$	$E_c - 0.16$	$E_c - 0.5$[a]
Trap density N_T (cm^{-3})	4.6×10^{12}	6.5×10^{12}	1.3×10^{12}	4.9×10^{12}	3.5×10^{13}
Capture cross-section σ (cm^2)	1.39×10^{-14}	5.7×10^{-15}		1.2×10^{-18}	

[a] Estimated value based on a approximated estimation of the position of the DLTS peak.

Table 2
Summary of the DLTS and C–V analysis for the EPV and NREL CIGS cells

	EPV CIGS cell	NREL CIGS cell		
Approximate peak temperature (K)	270	100	250	335
Activation energy (eV)	$E_v + 0.94$	$E_c - 0.07$		
DLTS peak sign	–	+	+	+
Trap carrier type	Majority	Minority	Minority	Minority
Net hole density N_a (cm^{-3})	3×10^{15}	2.25×10^{15}		
Trap density N_T (cm^{-3})	6.5×10^{13}	4.2×10^{13}		
Capture cross-section σ (cm^2)		6×10^{-18}		

some defect structures is so small that little increase in thermodynamic potential results, and hence there is insufficient driving force to ensure their elimination under many synthesis conditions. The reported formation energies of the deep-level defects in the CIS and CIGS absorbers are in the order $V_{Cu} < In_{Cu} < Cu_{In} \approx In_{Cu} < V_{Se}$ [1,18]. However, the defect distribution depends significantly on the stoichiometry. A more detailed investigation of the nature of deep-level defects and their role on the recombination process and performance in the CIS and CIGS films could further elucidate the material behavior and contribute to improving the performance of CIS-based cells.

Acknowledgements

This work was supported under the DOE/NREL Thin Film Photovoltaics Partnership Program (*TFPPP*) and monitored by NREL under subcontract No. XAF-8-17619-32. The authors would like to thank Dr. Bolko Von Roedern and Dr. Martha Symko-Davies of NREL for their interest and support of this work. The CIGS samples used in this study are provided by the NREL and EPV Inc.

References

[1] Zhang SB, Wei S-H, Zunger A. Phys Rev B 1998;57(16): 9642–51.
[2] Schön JH, Bucher E. Solar Energy Mater Solar Cells 1999; 57:229–37.
[3] Neumann H, Tomlinson RD. Solar Cells 1990;28:301–7.
[4] Deibel C, Wessel A, Dyakonov V, Parisi J, Palm J, Karg F. Thin Solid Films 2003;431–432:163–6.
[5] Christoforou N, Leslie JD, Damaskinos S. Solar cells 1989;26(3):197–214.
[6] Igalson M, Zabierowski P. Thin Solid Films 2000;361–362: 371–7.
[7] AbuShama J, Johnston S, Ahrenkiel R, Noufi R. In: Proceedings of 29th IEEE Photovoltaic Specialist Conference. New Orleans; 2002.
[8] Lang DV. J Appl Phys 1974;45:3023.
[9] Mitonneau A, Martin GM, Mircea A. Inst. Phys. Conf. Ser. vol. 33a. 1977. p. 73.
[10] Schroder DK. Semiconductor Material and Device Characterization. New York: John Wiley & Sons Inc; 1998.
[11] Li Sheng S. Semiconductor Physical Electronics. New York and London: Plenum Press; 1993.
[12] Stanbery BJ, Chang C-H, Kim S, Kincal S, Lippold G, Ahrenkiel SP, Kerr LL, Anderson TJ, Al-Jassim MM. Self organized processes in semiconductor alloys. In: MRS Symposium Proceedings, vol. 583. 2000. p. 195–200.
[13] Gödecke T, Haalboom T, Ernst F. Z Metallkd 2000;91(8): 622–62.
[14] Johnston SW, Ahrenkiel RK, Pak AJ, Friedman DJ, Kurtz SR. National Center of Photovoltaics (NCPV) and Solar Program Review Meeting. 2003.
[15] Versluys J, Clauws P, Nollet P, Degrave S, Burgelman M. Thin Solid Films 2003;431–432:148–52.
[16] Keyes BM, Dippo P, Metzger W, AbuShama J, Noufi R. In: Proceedings of the 29th IEEE Photovoltaic Specialists Conference. New Orleans (LA); 2002.
[17] Keys BM, Hasoon F, Dippo P, Balcioglu A. Abulfotuh F. In: Proceedings of the 26th IEEE Photovoltaic Specialists Conference. 1997.
[18] Neumann H, Kuhn G, Moller W. Physica Stat Sol (b) 1987;144:565.